The Cuban Scientist

Year 2023 Volume 4 | Issue 1

In this issue:

Quantum dynamics simulations using quantum trajectories

Lidice Cruz Rodriguez[a]

Department of Physics and Astronomy, University College London, Gower Street, London WC1E 6BT, UK

In this work we give a short overview of the hydrodynamic formulation of quantum mechanics, together with some examples of its application to quantum dynamics simulations using the Quantum Trajectory Method.

Investigating the real-time dynamics of many-body correlated systems is one of the major challenges in contemporary theoretical physics and chemistry. The full quantum-mechanical description requires the solution of the time-dependent Schrödinger equation (TDSE). The standard methods for exact numerical computations are based on spatial grids, basis sets of functions, or discrete variable representation. These methods have the disadvantage that while retrieving the full quantum mechanical solution, they scale exponentially with the system's dimensions, making them not applicable beyond ten degrees of freedom. In contrast, if we can treat them classically, the classical molecular dynamics methods (MD) allow modeling systems of thousands of particles by propagating ensembles of trajectories.

Therefore, looking for trajectory-based methods to perform quantum dynamics simulations is a very active field of research. A natural way of addressing this problem is to use quantum trajectories. An extended explanation of the fundamental principles and equations of this theory can be found in Ref. [1]. The starting point is expressing the wave function in terms of a real phase $S(x,t)$, and density $\rho(x,t)$,

$$\Psi(x,t) = \sqrt{\rho(x,t)}e^{iS(x,t))}. \tag{1}$$

The quantum trajectories are defined such that their velocity is,

$$\dot{x} := \left.\frac{\nabla S(x,t)}{m}\right|_x = x(t). \tag{2}$$

After substituting in the TDSE, this leads to a set of hydrodynamic equations,

$$\frac{dS}{dt} = \frac{1}{2}mv^2 - (V+Q)\ , \tag{3}$$

$$\frac{d\rho}{dt} = -\rho\frac{\partial v}{\partial x}\ , \tag{4}$$

$$m\frac{dv}{dt} = -\frac{\partial(V+Q)}{\partial x}\ . \tag{5}$$

The first two equations determine the time evolution of the hydrodynamic fields, and the last one is the equation of motion of the quantum trajectories. To solve them, we need the initial positions of the trajectories x_0 and the wave function Ψ_0 at $t=0$. The ensemble is initially distributed according to $|\Psi_0|^2 = \rho_0$, and their initial velocity is defined from Eq. (2). Under these conditions, the time evolution of the quantum trajectories renders the wave function $\Psi(x,t)$ at every time t. It is important to remember that this ensemble doesn't represent the actual material particle; each trajectory is a possible realization of a single particle. Eq. (3) is a Hamilton-Jacobi-like equation, but it has an additional term known as the quantum potential,

$$Q = -\frac{\hbar^2}{4m}\left(\frac{\nabla^2\rho}{\rho} - \frac{1}{2}\left(\frac{\nabla\rho}{\rho}\right)^2\right)\ , \tag{6}$$

which is the one bringing all the non-local effects to the dynamics. The gradient of this quantum potential is identified as the quantum force, and it enters the Newton-like equation (5) together with the classical force acting on the particles. Details about this theory and how the hydrodynamic equations are derived are given in Refs. [1] and [2].

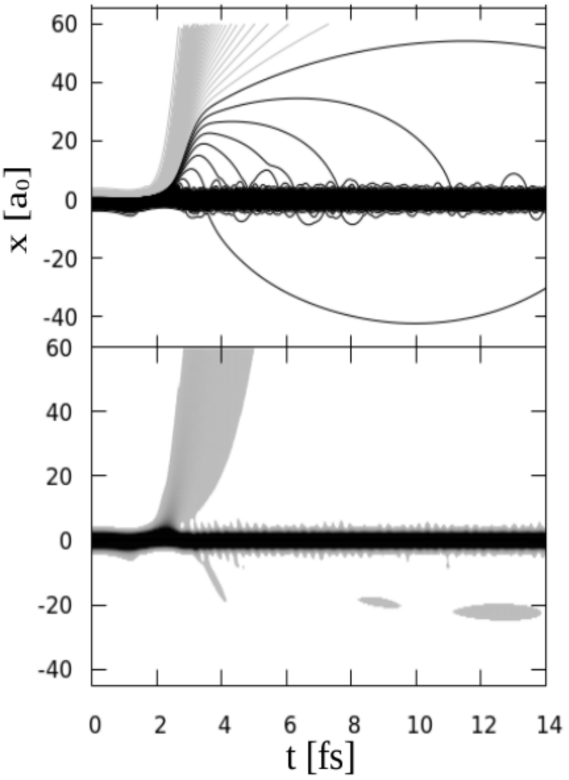

Figure 1: In the top panel we show the time evolution of an ensemble of $N = 501$ trajectories. In the bottom panel the time-dependent probability density evaluated via wave packet propagation is plotted. The figure was adapted from [5].

From the computational point of view, there are two ways of determining the time evolution of quantum trajectories. The first approach consists of solving the TDSE and, hence computing the trajectories. This leaves us with the problem we described initially, as we need to apply the standard and very computationally expensive methods to solve the TDSE.

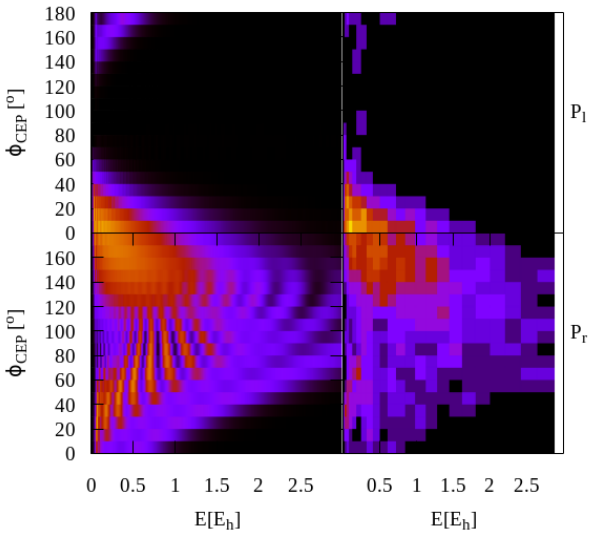

Figure 2: Density map of the left/right photo-electron spectra P_l (upper panel) and P_r (lower panel) as a function of energy and CEP parameter. The figure was taken from [5]

A different approach is based on using the trajectories as a tool to solve the Schrödinger equation. Using Eqs. (3)-(5), we can propagate the ensemble of trajectories together with the density and phase and build the wave function and any observable at every time step. A particular implementation of this approach was proposed in [3], and it is known as the Quantum Trajectory Method (QTM).

The QTM possesses many challenges from the computational point of view. One of the more important ones is evaluating the quantum potential and force at the trajectories as they form a very unstructured grid. An extended discussion about the QTM and its practical difficulties can be found in Ref [2].

In our work [4], we proposed an analytical approximation to the quantum potential and force valid for one-dimensional model systems. We applied the method to model the zero-point energy of harmonic and an-harmonic potentials and the real-time dynamics of bound and scattering problems. Furthermore, we study the laser-driven electron dynamics by strong and ultrashort laser pulses [5]. Here we will show some of the results of the latest application. More results and details about the implementation of the model and the pulse shape are given in our original publication [5].

In Fig. 1, the top panel shows the time evolution of an ensemble of $N = 501$ trajectories driven by the influence of a strong laser pulse. The bottom panel shows the results of a standard wave packet simulation used as a benchmark. The figure illustrates how the trajectories are a powerful tool to visualize the dynamics.

An interesting phenomenon to study with very short laser pulses is the impact of the Carrier Envelope Phase on the electron dynamics. In very short laser pulses, we can evaluate the asymmetry in the photo-electron spectra. The top panel of Fig. 2 shows the ionization probability (P_l) to the left, and the bottom panel the ionization probability (P_r) to the right. Within our trajectory-based approach, this is calculated by adding up how many trajectories end up in each direction. The results from our method are shown in the left column, while in the right column, we show the benchmark calculations.

Notes

a. Email: lidicecruzr@gmail.com

References

[1] P. R. Holland, The quantum theory of motion. Cambridge University Press, Cambridge, MA (1993).

[2] Lidice Cruz Rodríguez, Trajectory-based methods for the study of ultrafast quantum dynamics. PhD Thesis, Université Paul Sabatier - Toulouse III (2018).

[3] R. E. Wyatt, Quantum dynamics with trajectories. Springer Science & Bussiness Media (2006).

[4] Cruz Rodríguez, L., Uranga-Piña, Ll., Martínez-Mesa, A. and Meier C., Quantum dynamics modeled by interacting trajectories. Chemical Physics 503 (2018) 39-49.

[5] Cruz Rodríguez, L., Uranga-Piña, L., Martínez-Mesa, A., & Meier, C. Quantum trajectory study of laser-driven atomic ionization. Chemical Physics Letters, 715, (2019) 211-216.

Mycological Explorations of Southern United States: a Journey of Discoveries. Part 1

Gregorio Delgado[a]

Eurofins Built Environment, 6110 W. 34th St., Houston, TX 77092, USA

A summary of taxonomic and phylogenetic studies of saprobic microfungi collected in southern United States is presented. One novel genus and two species of asexual Ascomycota were described new to science from the southwestern states of Arizona and New Mexico.

Ascomycota is the largest phylum of the kingdom Fungi. Most of its members are filamentous and many of them are capable of reproducing both sexually or asexually. However, a large number of ascomycetes are known only by their asexual states and they are called anamorphic, mitosporic, conidial or asexual fungi. Their most common and morphologically diverse type of asexual propagule is the conidium, which is produced by mitosis on specialized conidiogenous cells born on modified hyphae named conidiophores and easily dispersed by wind and water splash. Ecologically, these fungi are often saprotrophs able to colonize a wide range of substrates and habitats in nature, actively participating in the decomposition and recycling of nutrients in ecosystems while releasing secondary metabolites and bioactive compounds with many different biotechnological, industrial and pharmacological applications. The systematic position of many of these asexual fungi is unknown due to the limitations of morphological and developmental characters to establish reliable phylogenetic relationships. DNA sequence data in combination with methods of statistical inference are used nowadays to incorporate them into the current classification of the Fungi.

On the other hand, the southern states of the United States, from California to the west to Florida in the southeast, include a wide spectrum of ecological regions encompassing tropical wet and eastern temperate forests, plains, deserts and forested mountains, as well as a variety of climates ranging from arid or semi-arid to humid subtropical and Mediterranean. The term 'southern' is not used here in a historical or geographical sense but applies to those states along the southern border or lining the Gulf of Mexico. Such a large and ecologically diverse region is expected to harbor a wide range of novel microscopic fungi belonging to the asexual Ascomycota, particularly those inhabiting dead plant debris and having a saprobic lifestyle.

The diversity of this group of microfungi has been systematically studied during the past nineteen years in collaboration with mycologists from Czech Republic, Germany, Japan, Mexico, Spain and United States. Several fieldworks were carried out in forested or suburban areas of Arizona, California, Florida and Texas with the aim to collect pieces of dead wood, branches, twigs, decaying bamboo culms, palm rachides, petioles, inflorescences, climbing vines and leaf litter among other substrates usually colonized by these microorganisms. Colonies were detected in the field using a hand lens and materials were brought to the laboratory for further processing. They were first washed-off under tap water and incubated in moist chambers at room temperature (23–25°C) to enhance growth and sporulation followed by periodical examinations under the stereomicroscope. Fungal structures were studied and measured under the light microscope (LM) at 1000× magnification. To obtain cultures, single-spore isolations were performed by picking-up conidia with a sterile needle and placing them aseptically on malt extract agar (MEA) or potato dextrose agar plates. For scanning electron microscopy (SEM), pieces of natural substrate or culture media with colonies were processed following standard sample preparation protocols. Voucher specimens and strains are deposited in international herbaria and culture collections. Genomic DNA was extracted from cultures using different protocols followed by PCR amplification and DNA sequencing of nuclear ribosomal and protein coding gene markers used nowadays in fungal phylogenetics studies. Methods of phylogenetic reconstruction such as Maximum Likelihood or Bayesian Inference were employed

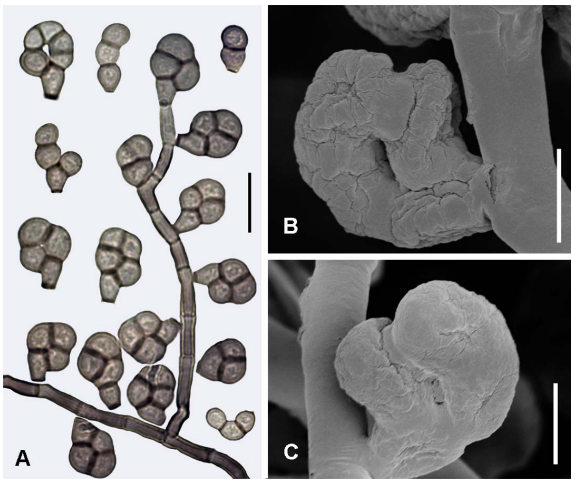

Figure 1: *Curviclavula anemophila*. Conidiophores, conidiogenous cells and conidia in LM (A) and SEM (B–C). Scale bars: A = 10 µm; B, C = 3 µm. Source [1]

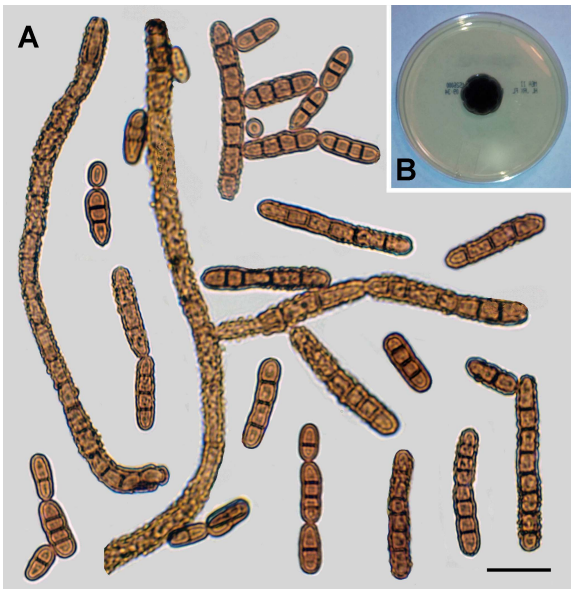

Figure 2: *Septonema lomanii*. Conidiophores, branches and conidia in LM (A) and (B) Colony on MEA. Scale bar: A = 20 µm; B = 1 cm. Source [2]

to infer relationships from molecular data and to estimate phylogenetic trees. Novel DNA sequences were publicly deposited in GenBank.

Despite being popularly depicted as desertic or arid states, Arizona and New Mexico both contain in the north large tracts of montane coniferous forest dominated by the widespread Ponderosa pine among other plant substrates suitable for the development of a rich saprobic mycobiota. Mycologically, however, microfungi have been relatively poorly explored compared with mushrooms or lichenized fungi. As a result of studying samples from these areas, distinct morphological, cultural and molecular characters led to the description of one novel genus, *Curviclavula*, and two new species named *C. anemophila* and *Septonema lohmanii*.

In the case of *Curviclavula*, the source colony was recovered from an air sample collected outdoors in northern New Mexico [1]. The fungus took its name from the peculiar club shape and unique development of its conidia (Figure 1). They resemble at first a tiny hand in side view, but the apical cells of the developing conidium later curves and fuses with the lateral and adjacent cells once they become in contact eventually forming a tightly appressed, subglobose to broadly club-like shaped conidium. Phylogenetic analyses of molecular data revealed a placement within the order Helotiales in the class Leotiomycetes and affinities for members of the family Hyaloscyphaceae.

Septonema lomanii, on the other hand, was collected independently in both northern Arizona and the Czech Republic on two different pine species [2]. The fungus is distinct among *Septonema species* by its heavily ornamented conidiophores, branches, conidia and hyphae, ranging from verruculose to strongly verrucose with prominent rounded warts and yellowish brown to brown or reddish brown in color (Figure 2). Multigene phylogenetic analyses suggested a placement within the Mytilinidiales belonging to the class Dothideomycetes and the first time a septonema-like fungus is linked to the order using molecular data. Based on morphological and molecular evidence, both the Arizona and Czech collections were considered conspecific despite their disjunct geographical distribution.

Future explorations will continue uncovering the outstanding diversity of microfungi in southern United States especially in poorly studied areas of the southwest with a variety of habitats and ecosystems.

Notes

a. E-mail: Gregorio.Delgado@et.eurofinsus.com

References

[1] Delgado, G., Miller, A. N. and Fernandez, F. A., *Curviclavula*, a new genus of anamorphic Helotiales (Leotiomycetes) isolated from air, *Mycological Progress* **14** (2015) 3 (1–7)

[2] Delgado, G., Koukol, O., Miller, A. N. and Piepenbring, M., *Septonema lohmanii*, a new species in Mytilinidiales (Dothideomycetes) and the phylogenetic position of *S. fasciculare*, *Cryptogamie Mycologie* **40** (2019) 3–21

Carbon Capture in Trees

Antonio Mijail Perez[a], Dora Pilar Maul, and Luis Alfredo Cendan

St. Thomas University, College of Health Sciences and Technology, Miami Gardens, FL. USA

Our project was conducted in Amelia Earhart Park, in the city of Hialeah, Florida, with the purpose of calculating the total amount of Biomass and Carbon Stock produced by trees in selected areas of Amelia Earhart Park.[b]

Introduction

The world's forests play a pivotal role in the mitigation of global climate change. Particularly, tropical forests have assumed increasing importance in international efforts to mitigate climate change thanks to their capacity to store carbon and because of the significant emissions caused by their destruction [2]. Researchers have strived to look for different ways to calculate the constant CO_2 emissions as well as carbon sequestration to find solutions to reduce the emission of greenhouse gases and manage the expanding climate change challenge.

Determination of carbon sequestration potential in terrestrial ecosystems through biomass estimation has been the most widely followed approach. Biomass is the measure of biological matter expressed in weight and can apply to individual trees or entire communities across a unit of area.

The urban environment presents important considerations for global climate change. Over half of the world's population lives in urban areas. The term "urban forest" refers to all trees within a densely populated area, including trees in parks, on streetways, and on private property. Though the composition, health, age, extent, and costs of urban forests vary considerably among different cities, all urban forests offer some common environmental, economic, and social benefits.

Our project was conducted in Amelia Earhart Park, in the city of Hialeah, Florida, with the purpose of calculating the total amount of biomass and carbon stock produced by trees in selected areas of the park, the contribution from hardwood trees and palm trees, and the amount of carbon dioxide that different tree species sequester from the atmosphere.

Materials and methods

Study site

The project was conducted in Amelia Earhart Park, City of Hialeah. The 515 acre (208.4 ha) park is situated just south of the Miami-Opa Locka Executive Airport and offers a series of recreational attractions together with wide green spaces with winding pathways beneath trees of over 20 different species. 40% of the park (83.4 ha) is land area, the rest is water parks and pools. We selected a 21 ha area (ca. 25% of the land area) in the park for sampling; an area that contains a diversity of tree species including hardwood trees and palm trees. Tree species were identified using taxonomical keys.

From Eq. (1)	
Mean	1209.654 03
St. Dev.	1569.247 74
Min.	33.559 734 9
Max.	13 883.8063
Sum	706 437.954
Count	584

Table 1: Overall biomass calculated.

From Eq. (1)	
Mean	568.537 394
St. Dev.	737.546 439
Min.	15.773 075 4
Max.	6525.388 96
Sum	332 025.838
Count	584

Table 2: Overall carbon stock calculated

Analysis

We measured Tree perimeters in centimeters using a Tailor's tape on hardwood tree species and palm trees, as a first step to determining their biomass. We also measured the height of the trees using a clinometer. We transformed perimeters (at breast height, i.e. 130 cm above the ground) into diameters. To determine biomass and carbon stock we used procedures and equations taken from the scientific literature. As already used in previous projects, equations are given by

$$Y = 21.297 - 6.953\ \mathrm{DBH} + 0.740\ \mathrm{DBH}^2 \quad (1)$$

$$\ln Y = e^{-1.716\ +\ 2.413 \ln \mathrm{DBH}} \quad (2)$$

for the Hardwood Trees, and

$$Y = 0.00388\ (\mathrm{DBH}^2)^{1.6063} \quad (3)$$

for the Palm Trees. In all the equations Y is the biomass, its units are $[Y] = Kg/\text{tree}$, and DBH stands for Diameter at Breast Height.

Stats	Eq. (1)	Eq. (2)	Eq. (3)
Mean	1426.95	2265.85	170.49
St. Dev.	1643.33	3079.46	145.98
Min.	35.68	60.55	33.56
Max.	13 883.81	28 081.96	1158.49
Sum	689 218.93	1 094 407.01	17 219.02
Count	483	483	101

Table 3: Basic statistics of biomass for all three formulas for hardwood and palm trees.

Stats	Eq. (1)	Eq. (2)	Eq. (3)
Mean	670.67	1064.95	80.13
St. Dev.	772.36	1447.34	68.61
Min.	16.77	28.46	15.77
Max.	6525.39	13 198.52	544.49
Sum	323 932.9	514 371.3	8092.94
Count	483	483	101

Table 4: Basic statistics of carbon stocks for all three formulas for hardwood and palm trees.

Analysis of Carbon Stock

We calculated the aboveground biomass, and carbon stock by assuming that the carbon content is approximately 47% of the total aboveground biomass [3, 4]

$$\text{Carbon} = \text{Biomass} \times 0.47 \tag{4}$$

The dataset obtained was analyzed to address the hypotheses of this study. All statistical analyses were conducted using the Data Analysis add-in in Excel and PAST.

Results

General results

Overall biomass was 706 437.95 kg (706.44 Mg), and overall, carbon stock was 332 026 kg (332.02 Mg). The area sampled constitutes around 25% of the park land area, so if we extrapolate to the whole land area of the park, we could say that the overall biomass would be roughly 2 825 751.80 kg (2825.75 Mg), and carbon ctock ca. 1 328 104 kg (1328.10 Mg). To calculate the totals, we only used equation (1), since it's the one that yielded the highest determination coefficient for this study ($r2 = 0.89$). See Table 1 and Table 2.

To express the results by units of area we made the following extrapolations. We know from the web that the total area for Amelia Earhart Park is 208.41 ha, of which, using Google Earth maps, we estimated that 40% is land area and the rest is water parks and pools. That 40% represents 83.36 ha of which we sampled ca. 25%, for an effectively sampled area of 20.84 ha. In conclusion, the total biomass calculated, expressed by area, is 33.9 Mg ha^{-1}, and the carbon stock is 15.93 Mg ha^{-1}.

Hardwood and Palm Trees

We collected information to support the importance of increasing the number of parks, and hardwood trees in urban environments that operate as "carbon sinks", and consequently carbon reservoirs. Total biomass for hardwood trees was 689 218.93 kg (689.22 Mg), and total biomass for palm trees, was 17 219.02 kg (17.22 Mg). See Table 3 and Table 4.

Differences in biomass based on allometric equations, as well as Donkor allometric equation for palm trees [3], are very significant ($T = 7.67$, $p < 0.01$). We obtained the same value in the T-test conducted between both carbon stocks compared, so differences are equally very significant.

Notes

a. Email: AntonioPerez@stu.edu

b. Original report on this study is Ref. [1]

References

[1] Perez A. M., Cendan L. & Maul DP., Biomass and Carbon Capture in Trees at Amelia Earhart Park, Miami Dade County, Florida, US, *European Journal of Environment and Earth Sciences* **3** 6 (2022) 18-22

[2] Brown S., & Iverson L. R., Biomass estimates for tropical forests, *World Resoures Review* **4** 3 (1992) 366–383

[3] Nogueira E. M., Fearnside P. M., Nelson B. W., Barbosa R. I. & Keizer E. W. H., Estimates of forest biomass in the Brazilian Amazon: new allometric equations and adjustments to biomass from wood-volume inventories, *For. Ecol. Manag.* **256** 11 (2008) 1853-1867

[4] Donkor E., Osei Jnr E. M., Prah B. E. K., Amoah A. S. & Mohammed Y., Estimation and Mapping of Carbon Stocks in Bosomkese Forest Reserve, *International Journal of Remote Sensing Applications (IJRSA)* **6** (2016) 41-52

Immunomodulating Activity of the Host Defence Peptides

Ernesto M. Martell[1], Melaine González-García[1], Ludger H. Ständker[2], and Anselmo J. Otero-González[a1]

[1]Center for Proteins studies, Faculty of Biology, Havana University, La Habana, Cuba
[2]Core Facility of Functional Peptidomics, Ulm University, Ulm, BW, Germany

Host defence peptides can complement the efficacy of conventional antibiotics amid the current strain resistance crisis. In addition to their microbicidal actions, they may have an immunomodulatory function, reinforcing an antimicrobial fight in a way that conventional antibiotics cannot efficiently address.[b]

The anti-infectious therapy is in a critical crossroad due to the resistance of emerging and reemerging pathogens to conventional antibiotics which are scarce in terms of new mechanisms of action. Host defence peptides (HDPs) including antimicrobial peptides (AMPs) are a promising option for their therapeutic potential because they exhibit a broad spectrum of activity against various infectious agents and they are less prone to provoke microbial resistance [1, 2, 3].

Immunomodulatory activity of HDPs has been recognized in the last 20 years as a promising field which has been in continuous growing. In a clear distinction to their direct antimicrobial killing actions, the immunomodulatory activities of host defence peptides are more effective in vivo. They offer a great opportunity for promising therapeutic applications in the fields of anti-infective therapy, chronic inflammatory diseases treatment, novel vaccine adjuvants development and anticancer immunotherapy.

These immune related functions of HDPs includes chemoattraction of leukocytes, modulation of inflammation enhancement of antigen presentation and polarisation of adaptive immune responses [4].

The complex mechanisms on which these activities are based are not fully understood and may be different for each HDP [5] which also is applied to the innate defence regulatory peptides (IDR) [6]. Previous studies suggest that the mechanism of action of the immunomodulatory activities of some of them on immune cells could be shown in Fig. 1.

Realising and maximising the therapeutic potential of these peptides requires a shift in perspective in HDP development [7]. Each immunomodulatory activity of HDPs can be linked to specific applications and they can work together to enhance their effects, as shown in Fig. 2.

The ability of immunomodulatory HDPs to promote anti-inflammatory cytokine production while exhibiting anti-infective activities reduces the development of excessive inflammation. This clearly represents an advantage compared to most immunostimulatory drugs, which commonly increase the production of proinflammatory cytokines and increase the risk of inflammatory

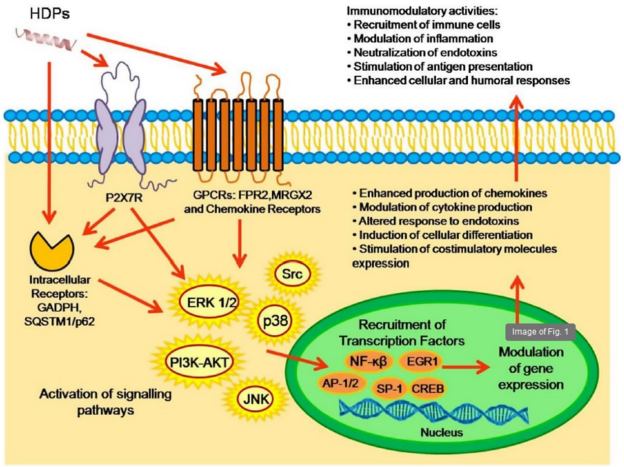

Figure 1: Overview of the mechanism of action of immunomodulatory HDPs in immune cells based on the mechanisms of LL37, human defensins and IDRs (Source: Reference [4]).

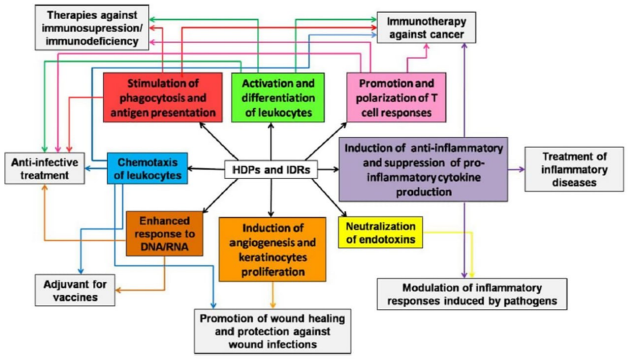

Figure 2: Connection between the main immunomodulatory activities of HDPs and IDRs and their potential therapeutic applications. Each immunomodulatory activity is represented with a specific color (Source: Reference [4]).

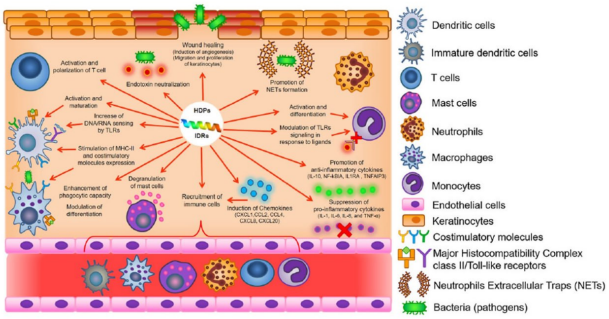

Figure 3: Immunomodulatory activities of HDPs/ IDRs against infections. HDPs exhibit a broad range of immunomodulatory activities that work together during infections to enhance immune response (Source: Reference [4]).

lesions [4]. Figure 3 shows the immunomodulatory activities of HDPs discussed above and how they work together in the context of infection.

The wide range of immunomodulatory activities of HDPs underlines their key role in immunity. In the context of the immune response, they promote immune cell recruitment, antigen presentation, and adaptive responses. It is known that in living organisms all the immunomodulatory effects of HDPs act simultaneously, connecting many immunological networks.

However, to improve the development of natural HDPs and IDRs for immunomodulatory therapies, it is particularly important to clarify more aspects of their immune system-related activities and to consider a systemic view of their impact on human physiology.

This is crucial to reduce the potential adverse effects of these therapies and uncover potential new applications of the attractive and promising immunomodulatory side of the HDP coin.

Notes

a. Email: aoterogo@yahoo.com

b. Original version of this article is reference [4]

References

[1] González-García M. *et al*, Antimicrobial peptides and multiresistant respiratory infections, *Rev Cub Med Trop* **71** (2) (2019) e343

[2] Otero-González A.J. *et al*, Antimicrobial peptides from marine invertebrates as a new frontier for microbial infection control, *FASEB J* **24** (2010) 1320-1334

[3] López-Abarrategui C. *et al*, Cm-p5: an antifungal hydrophilic peptide derived from the coastal mollusk *Cenchritis muricatus* (Gastropoda: Littorinidae), *FASEB Journal* **29** (8) (2015): 3315-25

[4] Martell, E.M. *et al*, Host defense peptides as immunomodulators: The other side of the coin, *Peptides* **146** (2021), 170644

[5] Hilchie, A.L. *et al*, Immune modulation by multifaceted cationic host defence (antimicrobial) peptides, *Nat. Chem. Biol.* **9** (2013) 761–768

[6] Scott, M.G. *et al*, An anti-infective peptide that selectively modulate the innate immune response, *Nat Biotechnol* **25** (2005) 465-472

[7] Nicholls E.F. *et al*, Immunomodulators as adjuvants for vaccines and antimicrobial therapy, *Ann. N. Y. Acad. Sci.* **1213** (2010) 46–61

Uncovering the biodiversity of root endophytic fungi in Europe

Gregorio Delgado[1] and Jose G. Maciá-Vicente[2]

[1]Eurofins Built Environment, 6110 W. 34th St., Houston, TX 77092, USA
[2]Department of Microbial Ecology, Netherlands Institute for Ecology (NIOO-KNAW), P.O. Box 50, 6700 Wageningen, The Netherlands

Extensive sampling of root endophytic fungi across Europe led to the discovery of two novel fungal genera, Endoradiciella *and* Extremopsis*, and the description of six species new to science.*

Endophytic fungi are an ecological group of endosymbionts capable of colonizing the internal tissues of plants without causing any visible symptoms. They can be present in any part of the plant host such as roots, leaves and stems during their whole life cycles or for certain periods only. Plants acquire their endophytes through horizontal transmission via asexual propagules produced by the fungus and spread out across the plant population or by vertical transmission to the plant offspring via the host seeds. They contribute to the plant fitness and performance by increasing their tolerance and adaptation to several biotic and abiotic stressors such as plant pathogens, drought, high soil salinity or extreme temperatures, while producing bioactive compounds and metabolites with many potential applications [1]. Phylogenetically, fungal endophytes are a highly diverse, polyphyletic assemblage of taxa mainly belonging to the phylum Ascomycota, and this peculiar lifestyle is known to have evolved multiple times within distantly related lineages of the kingdom Fungi.

During extensive sampling events for root endophytic fungi across Europe, a large number of isolates were obtained from surface-sterilized root pieces of different plant hosts. They were grouped into operational taxonomic units (OTUs) after sequencing their nuclear ribosomal DNA internal transcribed spacer region (ITS) followed by comparison with reference databases. Poorly represented OTUs usually consisting of one or a few isolates or those taxonomically assigned to rare species were subjected to further blast searches in GenBank to confirm their initial identification. If their percent identity was low or below a certain threshold, they were selected for further investigation. Isolates were plated in different agar media to study their morphological and cultural features and to induce sporulation. None of them, however, sporulated in any of the media used and they were considered sterile. Besides their ITS, other gene markers used nowadays in fungal identification were sequenced for novelty confirmation and comparison with those available in GenBank. Strains were deposited at the culture collection of the Westerdijk Fungal Biodiversity Institute (CBS) in The Netherlands and novel DNA sequences were deposited in GenBank.

As a result, two novel endophytic genera, *Endoradiciella* and *Extremopsis*, and six species, *Cyphellophora endoradicis*, *Endoradiciella communis*, *Extremopsis radicicola*, *Halocryptovalsa endophytica*, *Hymenoscyphus radicis* and *Tetraploa endophytica*, were described new to science from root samples obtained in Spain, Germany, France and Croatia.

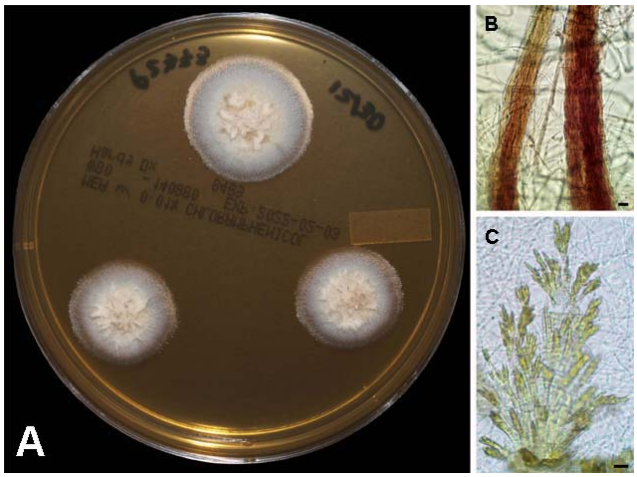

Figure 1: *Endoradiciella communis*. Colonies on MEA after 2 weeks at 25°C in surface view (A). Hyphal cords (B). Bundles of needle-shaped crystals (C). Scale bars = 10 µm. Source [2]

A first example of a root endophytic novelty discovered in Europe is *Endoradiciella*. The fungus is represented by its type species, *E. communis*, which was isolated from roots of *Microthlaspi perfoliatum* and *M. erraticum* (Brassicaceae) in France and Germany, respectively [2]. Mycelium is composed of hyphae often aggregated in tightly packed, reddish brown hyphal cords and produces greenish yellow bundles of needle-shaped or thin rectangular-bladed crystals on malt extract agar (MEA) after two months of incubation (Figure 1). Curiously, multigene phylogenetic analyses revealed that the three recovered strains of *E. communis* formed a well-supported lineage with fifteen other isolates available in GenBank and annotated as Helotiaceae sp. or Helotiales sp. They all share a similar root endophytic lifestyle and their ITS sequences are identical or almost identical to those of *Endoradiciella*, suggesting they might be conspecific. Most of them were isolated from several locations all over Europe including Bosnia & Herzegovina, Croatia, France or the

UK and the reason of the specific epithet of the fungus *'communis'* or widespread. They clustered within the family Porodiplodiaceae belonging to the order Helotiales of the class Leotiomycetes.

Another example of a novel root endophyte is *Extremopsis*, based on *Ex. radicicola* as the type species, and isolated from surface-sterilized, asymptomatic roots of an *Arabidopsis thaliana* (Brassicaceae) plant inoculated with soil originated from wet heathlands in Spain [3]. The three recovered strains of the fungus did not sporulate in any of the different culture media used including MEA, Potato Dextrose Agar, Modified Cellulose Agar or Water Agar supplemented with wooden toothpicks, but they produced abundant chlamydospores in all media (Figure 2). Phylogenetically, they grouped together in a strongly supported monophyletic lineage within the family Extremaceae belonging to the order Mycosphaerellales of the class Dothideomycetes. Similar to *Endoradiciella*, two other strains represented in GenBank by their ITS sequences and obtained from soil samples in Austria and Germany also clustered within the *Extremopsis* clade in multigene phylogenetic analyses. This suggests that they are conspecific with *Ex. radicicola* and the known distribution of the genus is therefore expanded from southern Spain to other localities across Europe.

A last example is the novel species *Halocryptovalsa endophytica*, isolated from surface-sterilized, asymptomatic roots of a wild plant of *Salicornia patula* (Amaranthaceae) in Spain [4]. This is a halophyte host which is well adapted to conditions of high salinity and common in saline ecosystems of the Mediterranean region. The two previously described species of *Halocryptovalsa* were also found associated with this type of host in marine environments but *H. endophytica* is the first member of the genus with an endophytic lifestyle. The two recovered strains of the fungus grouped together in a strongly supported monophyletic clade with a third isolate identified as '*Libertella* sp. F6' and represented in GenBank by an unpublished ITS sequence. This other isolate was originally obtained in Iran from another halophyte, *Juncus acutus*, and therefore it could be considered conspecific with *H. endophytica* based on molecular and ecological evidence. Multigene phylogenetic analyses placed the fungus within the family Diatrypaceae belonging to the order Xylariales of the class Sordariomycetes.

The examples outlined above show how fungal endophytes, despite being extensively studied nowadays, still represent a largely untapped reservoir of biodiversity awaiting to be discovered and it is our goal to continue describing them in the near future.

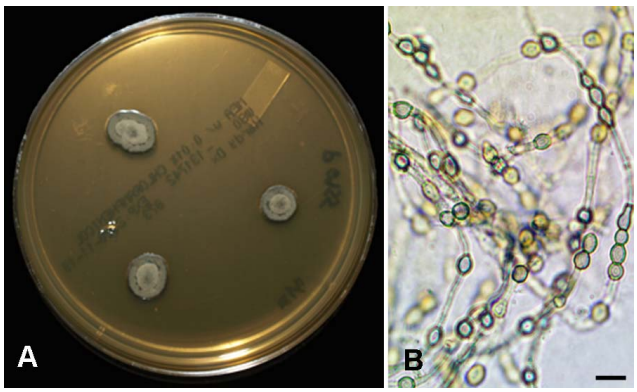

Figure 2: *Extremopsis radicicola*. Colonies on MEA after 3 weeks at 25°C in surface view (A). Chlamydospores (B). Scale bar = 10 µm. Source [3]

References

[1] Lugtenberg, B.J.J., Caradus, J.R. and Johnson, L.J., Fungal endophytes for sustainable crop production *FEMS Microbiology Ecology* **92** (2016) 1–17

[2] Delgado, G. and Maciá-Vicente, J.G., *Endoradiciella communis* gen. & sp. nov. Fungal Planet 1409. pp. 314–315. In: Crous et al. Fungal Planet description sheets: 1383–1435. *Persoonia* **48** (2022) 261–371

[3] Delgado, G. and Maciá-Vicente, J.G., *Extremopsis radicicola* gen. & sp. nov. Fungal Planet 1250. pp. 462–463. In: Crous et al. Fungal Planet description sheets: 1182–1283 *Persoonia* **46** (2021) 313–528

[4] Delgado, G., Nau, T. and Maciá-Vicente, J.G., *Halocryptovalsa endophytica* sp. nov. Fungal Planet 1514. pp. 234–235. In: Crous et al. Fungal Planet description sheets: 1478–1549. *Persoonia* **50** (2023) 158–310

Energy scales and scalar evolutions on a string model

Nana Cabo Bizet[a]

Departamento de Física, División de Ciencias e Ingenierías
Universidad de Guanajuato, Loma del Bosque 103
37150, León, Guanajuato, México.

A scale separation between the space-time's and the internal dimensions's degrees of freedom can be obtained by adjusting the parameters of the string geometry. We describe this scale hierarchy and the cosmological evolution of the scalar fields for type IIB string theory on the geometry of the mirror quintic.[bc]

String Theory is a strong candidate to a quantum gravity. In its realm one encounters the gauge interactions: electromagnetism, weak and strong, together with gravity at the Planck scale $M_{Pl} = \sqrt{c^5\hbar/G_N} \sim 10^{-33}$cm. This is the natural scale of a quantum gravity theory depending on the speed of light c, Planck's constant $\hbar$ and Newton's constant G_N. Calabi-Yau (CY) manifolds [2] constitute the extra dimensions of string theory, giving rise to 4-dimensional field theories with one supersymmetry. The CY geometries possess parameters: of shape (complex structure) and size (Kähler structure) denoted moduli.

We will study type IIB string theory with internal dimensions on the mirror of the quintic CY. This geometry is obtained by modding out a ${\mathbb{Z}_5}^3$ symmetry from a one-parameter family of polynomials on $\mathbb{P}^4$ [2]. This family is given by

$$W_\psi = \Big\langle \sum_k {x_k}^5 - 5\psi \prod_k x_k = 0, (x_1, \ldots, x_5) \in \mathbb{P}_4 \Big\rangle. \tag{1}$$

The ${\mathbb{Z}_5}^3$ symmetry is generated by phase rotations on the coordinates: $x_l \to e^{2\pi g(i) i/5} x_l$, with $l = 1, ..., 5$ and $g(1) = (0, 1, 0, 0, 4)$, $g(2) = (0, 0, 1, 0, 4)$, $g(3) = (0, 0, 0, 1, 4)$. The symmetry is modded out to obtain the geometry we will employ, the mirror quintic: $W_\psi/{\mathbb{Z}_5}^3$ [2]. The complex structure moduli space $z = (1 - \psi^{-5})$ of a given CY manifold has generic critical points: the conifold, the orbifold and the large complex structure point [1, 2]. In figure 1 the moduli space of the geometry is represented. There are three critical points.

The solution of the Einstein equations in multiple dimensions leads to a warped metric for the space-time that preserves Poincaré symmetry [3]

$$ds^2 = e^{2A(y)} \eta_{\mu\nu} dx^\mu dx^\nu + e^{-2A(y)} g_{mn} dy^m dy^n. \tag{2}$$

The hierarchy between the spacetime (4D) and compactification (6D) physical scales are given by the distance of the complex structure vacuum z_0 to the conifold as $e^A \sim z_0^{1/3}$ [2, 3]. We consider a so called no-scale potential, where the Kähler moduli ϕ^n are un-stabilized and satisfy the restriction: $K^{m\bar{n}} D_m W D_{\bar{n}} \bar{W} - 3|W|^2 = 0$. The effective theory possesses one local supersymmetry, meaning that it constitutes an $\mathcal{N} = 1$ 4D supergravity. The scalar potential, which we consider positive definite, can be written as

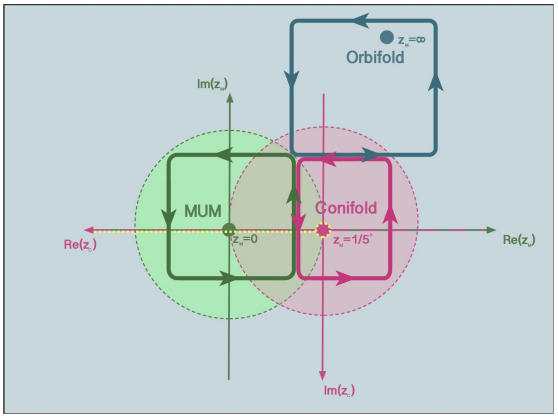

Figure 1: Moduli space of the mirror quintic Calabi-Yau 3-fold, with three critical points. Those points are parameter values at which the geometry develops a singularity.

$$V(\tau, z, \phi^i) = \frac{1}{2\kappa_{10}^2 g_s} e^K \left[K^{a\bar{b}} D_a W \overline{D}_{\bar{b}} \overline{W} \right], \tag{3}$$

where g_s is the string coupling constant and $\kappa_{10}^2 = \frac{{l_s}^8}{4\pi}$ with l_s the string length. V depends on the superpotential W and the Kähler potential K. The indices a and b denote the moduli fields. In this case we have two complex moduli fields: axio-dilaton and complex structure, scalar fields that are modes with zero mass in the string spectrum. There is a metric in the space of fields with inverse given by $K^{a\bar{b}}$, this occurs because the kinetic term in the Lagrangian reads $K_{a\bar{b}} \partial_\mu \phi^a \partial^\mu \bar{\phi}^b$. The quantity $D_a W = \partial_a W + \partial_a K W$ constitutes the susy covariant derivative. The superpotential [5] and Kähler potential read:

$$\begin{aligned} W &= \int_{CY} G_{(3)} \wedge \Omega = (F - \tau H) \, \Sigma \, \Pi \,, \\ K &= -\ln\left[-i\,(\tau - \bar{\tau})\right] - \ln\left[-i\,\bar{\Pi}^T \, \Sigma \, \Pi\right] - 2\ln\left[\mathcal{V}\right] \,, \end{aligned} \tag{4}$$

Every CY manifold with 3 complex dimensions has an holomorphic nowhere-vanishing 3-form. One can construct periods $\Pi(z) = \int_A \Omega$ as integrals of the holomorphic 3-form Ω on the 3-cycles. Cycles are dimension-3 sets of submanifolds of the CY with no boundary. Periods satisfy differential equations, denoted by Piccard-Fuchs (PF) equations [2].

Scale hierarchies

Here we describe the techniques employed to find Minkowski vacua and to evaluate their scale hierarchies. We obtain a formula for the vacuum expectation values of the axio-dilaton and the complex structure, for vacua solutions of the scalar potential (3). Minkowski vacua require the vanishing of both convariant derivatives $D_\tau W = D_z W = 0$. These formulas are solved simultaneously to obtain

$$\tau(z) = \frac{F\Sigma\bar{\Pi}}{H\Sigma\bar{\Pi}} = \frac{F\Sigma(\widetilde{\Pi}\Sigma\bar{\Pi})}{H\Sigma(\widetilde{\Pi}\Sigma\bar{\Pi})}. \tag{5}$$

Solving this equation one can find generic Minkowski vacua. We do so considering as many terms in the period series expansion, in order to reach convergence. The approximate value of the complex structure z_0 for a vacuum near the conifold is obtained to leading order as

$$\tau_0 = \frac{F\Sigma\bar{\Pi}^0}{H\Sigma\bar{\Pi}^0}\,, \qquad W_0 = (F - \tau_0 H)\Sigma\Pi^0\,. \tag{6}$$

The solution for a particular set of non-zero fluxes F_1, H_3, H_4 is obtained to be

$$z_0 \sim \exp\frac{H_3\partial\Pi_1\bar{\Pi}_3}{H_4\beta\bar{\Pi}_2}. \tag{7}$$

We found in [1] a correction to the hierarchies of [3]. The result is due to the compactness, as well as from considering the complete period series. Adjusting the fluxes, the warping parameter can lead to big hierarchies.

Scalar field evolution

We analyze the cosmological multifield evolution of the scalar fields τ and z. The setup is the Friedmann–Lemaître–Robertson–Walker background in space-time. One can compute parameters ϵ and η. Their size determines in which regions there can be scalar field displacements that fulfill a slow-roll evolution. These parameters are given by

$$\epsilon = \frac{K^{i\bar{j}}\nabla_i V\bar{\nabla}_j V}{V^2}, \tag{8}$$

$$\eta = \text{min eigenvector}\frac{K^{i\bar{j}}\nabla_i\bar{\nabla}_j V}{V^2}. \tag{9}$$

We computed them numerically in terms of the scalar potential (3). There are configurations of fluxes for which large inflationary regions with $\epsilon \ll 1$ and $\eta < 1$ are encountered. The results for a particular flux configurations are shown in figure 1. In all of the explored examples, the possible scalar field displacements are below the Planck scale, fulfilling the recent bounds obtained by the discussions of the species scale [4]. This indicates that the scalar potentials dicsussed are valid as an effective theory of strings, without incorporating higher oder curvature contributions.

Conclusions

We explored a string theory model. First we studied the existence of vacua solutions with a scale hierarchy between the internal and the space-time scale. We checked that they appear in the compact case, near conifold sigularities, finding a correction with respect to the generic argument, which can be of more than an order of magnitude. We determined that for the multi-field evolution the scalar field displacements are bounded by M_{Pl} in agreement with the recently discussed bound of the species scale [5]. These compactifications constitute a fertile realm of the string landscape, with potential applications to cosmological models.

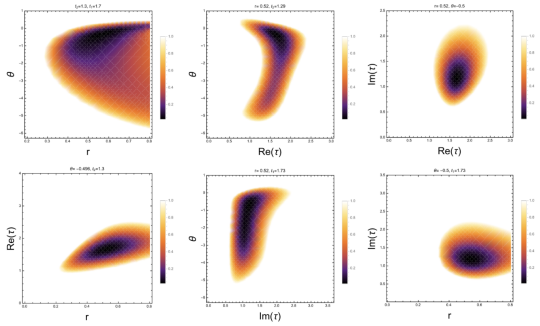

Figure 2: The evolution of the multi-field potential agrees with the so called bound of the species scale. The width of the flat regions is given by: $\Delta\phi_r = 0.124M_{pl}$, $\Delta\phi_\theta = 0.58M_{Pl}$, $\Delta\phi_{\tau_1} = 0.69M_{Pl}$, $\Delta\phi_{\tau_2} = 0.65M_{Pl}$.

Notes

a. Email: nana@fisica.ugto.mx

b. The research work of this note can be found in Ref. [1]

c. I thank the Isaac Newton Institute for Mathematical Sciences, Cambridge, for support and hospitality during the programme "Black holes: bridges between number theory and holographic quantum information" where this work was written. This work was supported by EPSRC grant no EP/R014604/1, U. of Guanajuato grants CIIC 264/2022 and CIIC 224/2023 and CONAHCyT grant A-1-S-37752. I acknowledge the ICTP Associates Programme (2023-2029).

References

[1] N. Cabo Bizet, O. Loaiza-Brito and I. Zavala, Mirror quintic vacua: hierarchies and inflation, *JHEP* **10** (2016) 082

[2] P. Candelas and X. C. de la Ossa, P. S. Green and L. Parkes, A pair of Calabi-Yau manifolds as an exactly soluble superconformal theory, *Nucl. Phys. B* **359** (1991) 21-74

[3] S. B. Giddings, S. Kachru and J. Polchinski, Hierarchies from Fluxes in String Compactifications, *Phys. Rev. D* **66** (2002) 16006

[4] D. Heisteeg, C. Vafa and M. Wiesner, Bounds on Species Scale and the Distance Conjecture, *Fortsch. Phys.* **71** (2023)

[5] S. Gukov, C. Vafa and E. Witten, CFT's from Calabi-Yau four-folds, *Nucl. Phys. B* **548** (2000) 69-108

New string symmetries

Nana Cabo Bizet[a]

Departamento de Física, División de Ciencias e Ingenierías
Universidad de Guanajuato, Loma del Bosque 103
37150, León, Guanajuato, México.

We study novel non-Abelian dualities between gauged linear sigma models, which constitute an ultraviolet description of string theory. These dualities can lead to new physical symmetries between different geometries.[b] [c]

Introduction

Dualities and symmetries relate different corners of string theory. In particular, Mirror Symmetry relates type IIA and type IIB string theories on mirror Calabi-Yau (CY) manifolds. On the other hand, T-duality constitutes a symmetry of string theory with one extra dimension on a circle with radius R, under the exchange $R \to \alpha'/R$. The process of considering a compact dimension is called a compactification. Mirror symmetry exchanges string modes that wrap the extra dimension with modes that posses linear momentum [4]. Additionally, mirror symmetry exchanges Kähler deformations with complex deformations on mirror manifolds. The former constitute parameters that set the sizes of the extra dimensions, whereas the latter constitute parameters that set their shape. Mirror symmetry is related to T-duality. It has been proved that mirror symmetry is a consequence of T-Duality in Gauged Linear Sigma Models (GLSMs) [3]. The GLSMs in 2D with $(2,2)$ supersymmetry (SUSY) are a powerful tool to describe strings propagating in a Kähler manifold (extra dimensions) [2]. SUSY exchanges bosons and fermions, permuting the spin statistics but leaving the action of the theory invariant. Under the renormalization group, i.e. the energy flow, the GLSMs have infrared fixed points with conformal invariance. These are non linear sigma models (NLSMs) which constitute world-sheet string theories. This means that GLSMs constitute an ultraviolet (UV) description of string theory.

We want to identify distinct geometries of string theory related by Abelian and non-Abelian T-dualities on GLSMs. We have developed a procedure to implement T-dualities in models with global symmetries [1]. It reproduces the standard Mirror Symmetry for the cases of Abelian global symmetries [3]. It also leads to geometrical generalizations. The following diagram shows the outline of our work:

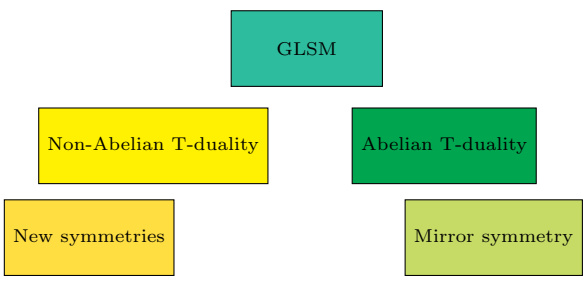

We are considering GLSMs with global symmetries, and implementing Non-Abelian T-dualities in order to obtain new symmetries of string theory, relating apparently distinct geometries.

There are different motivations to explore new symmetries of GLSMs. On one hand, Non-abelian GLSMs [5] provide – for the extra dimensions – more general ambient spaces than toric varieties. CY manifolds in these spaces are related to determinantal, Grassmanian, Pfaffian and more general non-complete intersection varieties [5]. A proposal for non-Abelian GLSMs mirror pairs have been presented in [6], which could be connected to non-Abelian T-dualities. It is also estimated that the class of non-complete intersections CYs [7] is much bigger than the class of complete intersections CYs.

Dualization of gauged linear sigma models

Our work consists of implementing T-dualities in sigma models with global symmetries, which could be Abelian and non-Abelian. The key observation is that a dualization procedure leads to a single Lagrangian that upon integration over two different subsets of fields conducts to dual field theories. We start with a reduction to 2d of 4d $U(1)$ gauge field theory with $\mathcal{N}=1$ SUSY. This dimensional reduction gives rise to a supersymmetric theory with two left and two right supersymmetries, i.e. $\mathcal{N}=2$ (2,2) 2d theory.

The supersymmetry can be implemented by defining superspace coordinates $x^\mu, \theta^\alpha, \bar{\theta}^{\dot{\alpha}}$. The first are the space-time coordinates with indices $\mu = 0,3$ and the second and third are anticommuting Grassman numbers with indices $\alpha = 1,2$, $\dot{\alpha} = 1,2$. The fermion indices can be also expressed as $\pm$ with $(\theta^1,\theta^2) = (\theta^-,\theta^+)$ and $(\theta_1,\theta_2) = (\theta_-,\theta_+)$. One can construct generators that transform the fields $(Q_\alpha, \bar{Q}_{\dot{\alpha}})$, and covariant derivates that act on the fields, given by $D_\alpha = \frac{\partial}{\partial\theta^\alpha} + i\sigma^\mu_{\alpha\dot{\alpha}}\bar{\theta}^{\dot{\alpha}}\frac{\partial}{\partial x^\mu}$ and its conjugate $\bar{D}_{\dot{\alpha}} = -\frac{\partial}{\partial\bar{\theta}^{\dot{\alpha}}} - i\sigma^\mu_{\alpha\dot{\alpha}}\theta^\alpha\frac{\partial}{\partial x^\mu}$. We employ the language of superfields in $\mathcal{N}=1$ SUSY in 4D. These superfields have as components the standard fields, which are related by SUSY transformations. There are different representations, and among them there are chiral superfields (csf) $\bar{D}_{\dot{\alpha}}\Phi = 0$, antichiral superfields (acsf) $D_\alpha\bar{\Phi} = 0$ and vector superfields (vsf) $V^\dagger = V$. Twisted-csf satisfy $D_+X = \bar{D}_-X = 0$ and the twisted-acsf satisfy

$\bar{D}_+\bar{X} = D_-\bar{X} = 0$.

The Lagrangian of a GLSM with gauge group $U(1)$ with vsf V_0 and N csfs Φ_i with charges Q_i can be written as [2]

$$L_0 = \int d^4\theta \Big(\sum_{i=1}^N \bar{\Phi}_i e^{2Q_i V_0}\Phi_i - \tfrac{1}{2e^2}\bar{\Sigma}_0\Sigma_0 \Big) \quad (1)$$
$$- \tfrac{1}{2}\int d^2\tilde{\theta} t\Sigma_0 + \text{c.c.},$$

where $t = r - i\theta$. The parameters of L_0 are the $U(1)$ gauge coupling e, the Fayet-Iliopoulos(FI) term r and the Theta angle θ.

We implement Abelian T-dualities in the GLSM in a distinct way to [4]. For mirror symmetry, the results coincide because the duality follows from the existence of a global symmetry. For two chiral fields with equal charge,the GLSM target-space is $\mathbb{CP}^1$ and the mirror dual manifold is the A_1-Toda variety.

Consider a particular case of (1), i.e., a GLSM with Abelian gauge group $U(1)$, N chiral superfields $\Phi_{k,i}$ with charges Q_k, $\sum_k n_k = N$, $i = 1, \ldots, n_k$ where n_k is the total number of chiral superfields with charge Q_k. There is a non-Abelian global symmetry $G = U(n_1) \times \ldots \times U(n_k)$, and a subset of it can be gauged to obtain the vsf V. By adding a Lagrange multiplier Ψ one gets a master Lagrangian

$$L_2 = \int d^4\theta \Big(\sum_k \bar{\Phi}_{k,i}(e^{2Q_k V_0 + V})_{ij}\Phi_{k,j} + \Psi\Sigma + \bar{\Psi}\bar{\Sigma} \Big)$$
$$- \int d^4\theta \tfrac{1}{2e^2}\bar{\Sigma}_0\Sigma_0 + \tfrac{1}{2}\Big(- \int d^2\tilde{\theta} t\Sigma_0 + \text{c.c.} \Big). \quad (2)$$

The original action is recovered by integrating out Ψ. Upon integration of the gauged vector superfield one obtains the dual model, leading to the following equations of motion: $(\bar{\Phi}e^{2QV_0}e^V T_a\Phi) = X_a + \bar{X}_a$. The relevant definition is $X_a = D_+\bar{D}_-\Psi_a + \{\chi, D_+\Psi_a\}$. For the case $\{\chi, D_+\Psi_a\} = 0$ the X_a is a tcsf, and $\bar{X}_a$ is an anti-tcsf.

Let us discuss the dualization of a simple case [1], when one has $SU(2)$ global symmetry. The original model has a $\mathbb{CP}^1$ vacuum. The dual effective scalar potential obtained from (2) after integrating the $U(1)$ gauge field in the Higgs branch is given by:

$$U = 2Q^2e^2|x_a n_a - t/(2Q)|^2 + B_a(x_a + \bar{x}_a), \quad (3)$$

where the x_a's are the scalar components of the tcsf. The constant B_a depends on the vector superfield components. After fixing the gauge, the new vacuum is parametrized by the two-dimensional space:

$$\sum_a x_a n_a = \frac{t}{2Q} - \frac{B_1}{2An_1},\ x_2 + \bar{x}_2 = x_3 + \bar{x}_3 = 0. \quad (4)$$

At the quantum level the theory has the symmetry $x_a \to x_a + \frac{2\pi i k_a}{2n_a Q}$, $k_a \in \mathbb{Z}$ coming from the periodicity of t, obtaining T^2 as the dual target space. For an Abelian direction inside of $SU(2)$ at fixed $n_a = \text{const}$, instanton corrections to the action are identified as $\tilde{W} = e^{-X_a n_a}$. Dual models are matched, by checking that the effective potential for the $U(1)$ gauged field is the same in both theories.

Conclusions

We developed a method to describe T-duality in SUSY $(2,2)$ 2D GLSMs. The Abelian T-duality gives rise to mirror symmetric models [3]. The non-Abelian T-dual theories give rise to new geometries [1]. For the case of a GLSM with $SU(2)$ global symmetry and geometry $\mathbb{CP}^1$, one obtains the dual geometry T^2.

There are many aspects of the dual geometries to be explored, for example: solving the duality for the full non-Abelian group. For instance, one has to determine the required non-perturbative effects on the dual theory, e.g. instanton effects. It would be relevant to compute the partition function with localization techniques. We also plan to dualize non-Abelian GLSMs, studying the connection between non-Abelian T-duality and Mirror Symmetry in Pfaffian and determinantal CY. It would be interesting to study compact geometries, i.e. a non-trivial superpotential in the original theory; and to perform a survey of dual geometries. We have studied new correspondences that can be relevant to explore the string theory landscape.

Notes

a. Email: nana@fisica.ugto.mx

b. The research work of this note can be found in Ref. [1]

c. I thank my collaborators: R. Díaz Correa, Y. Jiménez Santana, J. León Bonilla, A. Martínez Merino, L. Pando Zayas, R. Santos Silva and H. García Compeán. I thank A.Cabo Bizet for suggestions and corrections. I thank the INI, Cambridge, for support during the BLH programme. This work was supported by EPSRC grant no EP/R014604/1, UG grants CIIC 264/2022 and CIIC 224/2023, CONAHCyT grant A-1-S-37752 and the ICTP Associates Programme (2023-2029).

References

[1] N. Cabo Bizet, A. Martínez-Merino, L. A. Pando Zayas and R. Santos Silva, Non Abelian T-duality in Gauged Linear Sigma Models, *JHEP* **04** Issue (2018) 54

[2] E. Witten, Phases of N=2 theories in two dimensions, *Nucl. Phys. B* **403** (1993) 159-222

[3] K. Hori and C. Vafa, Mirror symmetry, arXiv:hep-th/0002222 (2000)

[4] T. H. Buscher, A Symmetry of the String Background Field Equations, *Phys. Lett. B* **194** (1987) 59-62

[5] K. Hori and D. Tong, Aspects of Non-Abelian Gauge Dynamics in Two-Dimensional N=(2,2) Theories, *JHEP* **05** (2007) 079

[6] W. Gu and E. Sharpe, A proposal for nonabelian mirrors, arXiv:1806.04678 (2018)

[7] F. Tonoli, Construction of Calabi-Yau 3-fold in P6, *Rend. Sem. Mat. Univ. Pol. Torino* **59** 2 (2001)

Do collaborative study habits shape personal epistemology?

Maybi Morell[a1], Rafael García[2], and Rogelio Diaz-Mendez[3]

[1]Lund University Cognitive Science, Lund University, 22100 Lund, Sweden
[2]Department of Physics, Technological University of Havana, La Habana, Cuba
[3]BA Cloud Software & Services - SSM, Ericsson AB, 16440 Kista, Sweden

We argue in favor of a positive answer to this question, providing evidence from the context of Cuban university students, where study groups form spontaneously at all academic stages. Personal epistemology, measured with a beliefs questionnaire, shows interesting behaviors as function of the group parameters.

In educational environments around the world, the phenomenon of students spontaneously forming groups for a myriad of activities is a common sight. Whether it's for social interaction, project collaboration, or academic study, these self-organized groups often serve as microcosms of teamwork and shared learning. This tendency is especially pronounced in the Cuban educational landscape, where the culture of communal learning is deeply rooted and widely embraced across all levels of academia. In Cuba, the practice of forming study groups is not just a casual or occasional occurrence; it's almost a cultural norm.

Instead of been formally organized or mandated by instructors, Cuban students typically take the initiative to create these groups themselves. They identify peers with whom they share academic goals or subjects of interest and come together to form a cohesive unit. Quite often, these groups are not just temporary alliances formed to tackle a specific assignment or prepare for an upcoming exam, but they remain stable throughout the entire academic year.

The stability of these self-formed study groups offers multiple benefits. It creates a consistent learning environment where students can rely on each other for academic support, exchange ideas, and challenge one another to achieve higher levels of understanding. This long-term stability also allows for the development of strong interpersonal relationships, which further enhances the group's effectiveness as a learning community.

While a substantial amount of research on collaborative learning has been centered around groups that emerge due to specific pedagogical strategies, there exists not much inquiry into study groups that forms autonomously, without any external prompting or intervention from educators. In our research these are termed as spontaneous small groups (SSGs). SSGs are intriguing because they provide a unique window into the world of collaborative learning, purely from the standpoint of the students. While external factors like the academic environment undoubtedly influence the formation of SSGs, the internal factors, specifically students' beliefs about knowledge and the learning process, might play a pivotal role.

On the other hand, the value of cooperative learning and group collaboration, has long been acknowledged for its benefits. It not only fosters socialization but also significantly enhances the learning process. Past research has consistently demonstrated that group discussions often yield better results than traditional lecture-based teaching. Such discussions stimulate critical thinking, facilitate personal and social adjustment, and are instrumental in altering attitudes. Within these group settings, students find it easier to dissect complex ideas, establish connections with previously acquired knowledge, and elevate their individual academic achievements. Recognizing these advantages, contemporary educational curricula are progressively emphasizing the importance of forming such study groups.

It is then only natural to be intrigued about the possible relationship that could exist between the epistemological beliefs held by the students and the specific features of the SSGs they belong to.

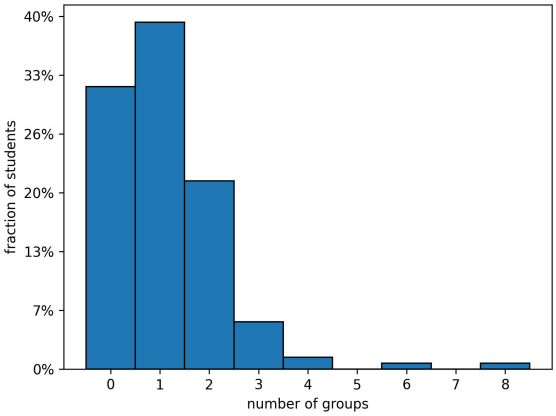

Figure 1: Multi-group preferences for the whole sample. The study found that most students were part of only one SSG. However, the size and number of these groups varied.

The concept of personal epistemology has been a focal point in the domains of cognitive and educational psychology for quite some time. Within the multidimensional paradigm it's posited that individuals cultivate their unique set of beliefs about knowledge and its learning process. These sets of beliefs, referred to as epistemological beliefs (EBs), offer profound insights

into how students perceive learning and knowledge. Over the years, various studies have pinpointed core beliefs within this framework. Some of these include beliefs about the structure of knowledge, its source, its certainty, as well as beliefs about the speed at which one can learn and the inherent ability to do so.

In 2021 we published a report [1] where a sample of 151 bio-medical engineering students was interviewed about study habits and EBs. Our study encompassed three distinct academic years, namely junior, intermediate, and senior. The students were surveyed to identify the SSGs and their EBs. The process of identifying spontaneous study groups was facilitated through a comprehensive survey, administered to all participants, in which they were asked to simply list their study mates. Following a cluster analysis, the groups were found and characterized, in particular regarding its size and distribution along the sample (see Fig. 1).

The epistemological beliefs were measured using a 34-item EBS questionnaire consisting of 34 statements. Students were asked to rate these statements on a 5 point Likert scale, ranging from 'strongly disagree' (1) to 'strongly agree' (5). The survey aims to assess various dimensions of students' beliefs about knowledge and learning. The answers were grouped into 10 subscales, which include beliefs like *Success is unrelated to hard work*, *Avoid integration*, *Do not criticize*, *Avoid ambiguity*, *Learning is quick*, *Knowledge is certain*, *Depend on authority*, *Seek single answers*, *Ability to learn is innate*, and *Learn the first time*.

These subscales were then analyzed to derive factors that represent the underlying epistemological beliefs of the students (see Table 1). A factor analysis was applied, leading to the identification of a four-factor structure for the epistemological beliefs. The four factors of EBs were named as: *Passive Learning*, *Certain Knowledge*, *Knowledge Handed down by Authority*, and *Quick Learning*. These factors accounted for 56.7% of the variance. The structure was subsequently validated using confirmatory factor analysis and the factors used to correlate with SSG variables.

Finally, the study found interesting relationships between EBs and SSGs. For students who studied alone (i.e., not part of any SSG), there was a tendency to have naive beliefs about Quick Learning. This suggests that the absence of group interaction may limit exposure to diverse viewpoints, thus affecting beliefs about the speed and nature of learning.

Correlations between EBs and SSGs were also found to differ depending on the academic year. For junior (second-year) students, a significant correlation was observed between the size of the study group and the belief that knowledge is handed down by authority. Specifically, the larger the group size, the more likely junior students were to hold this naive belief. This suggests that younger students in larger groups may be more susceptible to accepting information without critical evaluation. For senior (fourth-year) students, it was found that both the size and the number of SSGs were negatively correlated with the belief in Passive Learning. In other words, senior students who were part of larger and multiple study groups were more likely to have sophisticated beliefs about learning being an active process. This could indicate that as students gain academic experience, group study may play a role in fostering more complex and nuanced beliefs about learning and knowledge.

Subscale	Fac. I	Fac. II	Fac. III	Fac. IV
Success is unrelated to hard work	.708			
Avoid integration	.703			
Do not criticize	.612			
Avoid ambiguity		.671		
Learning is quick		.589		
Knowledge is certain		.568		
Depend on authority			.825	
Seek single answers			.504	
Ability to learn is innate				
Learn the first time				.879

Table 1: Higher loads for factors with eigenvalues greater than 1, subscales are built from the 34 items of the EBS. Factor I: Passive Learning; Factor II: Certain Knowledge; Factor III: Knowledge Handed down by Authority; Factor IV: Quick Learning

These findings reveal unexpected information about how beliefs and group dynamics are linked across different academic levels. For younger students, larger study groups were associated with less sophisticated views, specifically the belief that knowledge is simply passed down by authority figures. In contrast, older students in larger and multiple study groups exhibited more complex beliefs, particularly regarding learning as an active process. This surprising trend among younger students is examined through a sociological lens, hinting at the evolving nature of group interactions. As far as we're aware, this is a primary evidence to demonstrate that the size of study groups can either enhance or diminish the complexity of students' beliefs, depending on their academic stage.

Future research should delve deeper into the internal makeup of these groups to fully understand these outcomes. By gaining a solid understanding of these dynamics, educators are better positioned to devise pedagogical strategies that are more aligned with the students' individual and collective learning perspectives. Such alignment can potentially optimize the learning process, ensuring that students not only acquire knowledge but also develop greater understanding and appreciation of the learning journey.

Notes

a. Email: maybi.morell_ruiz@lucs.lu.se

References

M. Morell, R. García & R. Díaz-Méndez (2021). Personal epistemology and spontaneous small groups. *Educational Psychology* 41 (1) 99-112